High Stable Al-MCM-41: Structural Characterization and Evaluation for Removal of Methylene Blue from Aqueous Solution

Wafaa E. Rashwan[1] · Khaled S. Abou-El-Sherbini[2] · Mohammed A. Wahba[2] · Sohair A. Sayed Ahmed[1] · Peter G. Weidler[3]

Abstract

Aluminosilicate (Al-MCM-41) was synthesized via a modified wet-method in a Si/Al atomic ratio of 13.64:1.00 and calcination at 500 °C. The structural as well as the thermal stability were studied by powder X-ray diffractometry (XRD), thermogravimetric analysis (TGA), scanning electron microscope (SEM), Fourier transform infrared (FTIR) analysis and surface area measurements. Al-MCM-41 was confirmed to acquire a mesoporous structure with a high stability against hydrolysis which was attributed to the homogeneous dispersion of Al(III) in the silica framework. The adsorption parameters of the cationic dye methylene blue (MB), on Al-MCM-41 were investigated in aqueous solutions. The adsorption isotherm data showed a notable monolayer adsorption capacity (285 mg g^{-1}) of MB and fitted well the Langmuir adsorption model and the pseudo-second-order kinetics model. The adsorbent was applied successfully for removing 92.0–94.7% of MB from spiked fresh water samples and the initial capacity was recovered by 0.05 mol L^{-1} HCl or calcination.

Keywords Al-MCM-41 · Mesoporous · Adsorption · Kinetics · Methylene blue · Recovery

1 Introduction

Treatment of wastewater formed from different industries especially dyeing processes represents an obligatory process to save the critically limited fresh water resources from contamination [22]. Residual dyes inflict a severe hazard to the environment especially if discharged into water resources without treatment. This is because dyes are slowly biodegradable due to their complex molecular structures, which make them more stable and resistant to bio-degradation [31] and photo degradation as well [55]. Water contaminated with dyes may result in unhealthy effects such as vomiting, cyanosis, or haemolysis [47]. Therefore, many efforts are exerted to effectively remove cationic dyes from wastewater [41, 42, 67].

Generally, a variety of techniques including coagulation [26], flocculation [37], membrane separation [14] and adsorption [5, 41, 42, 50] have been utilized in removing of organic dyes. Among these varied techniques, the adsorption path combines the advantages of practical designing, regeneration and cost-effective application.

A successful adsorption removal encompasses some important aspects that adsorbent should fulfil such as: high adsorption capacity, reactivity, fast kinetics as well as high selectivity for adsorbates. Numerous solid materials including clays [34, 41], functional polymers [25, 30], activated carbon [27], and by-products [54] have been applied to adsorb dyes from wastewater. However, the low adsorption capacity and lack of recovery of most adsorbents limit their applications in removing dyes, especially at high concentration. High cost of some adsorbents like activated carbon also hinders their wide practical applications.

Mesoporous silica (MPS) [9, 53] and zeolite (ZT) [38, 59] are extensively effectively applied for removal of

✉ Mohammed A. Wahba
mohamedwahba12@gmail.com

1 Department of Physical Chemistry, National Research Centre, 33 El Bohouth St. (former Eltahrir St.), P.O. 12622, Giza, Dokki, Egypt

2 Department of Inorganic Chemistry, National Research Centre, 33 El Bohouth St. (former Eltahrir St.), P.O. 12622, Giza, Dokki, Egypt

3 Institute of Functional Interfaces, Karlsruhe Institute of Technology, 76344 Eggenstein Leopoldshafen, Germany

cationic hazards. Zeolite is preferred due to its better cationic exchange capacity (2.10–4.25 mEq/g) as it is composed of crystalline aluminosilicate TO_4 tetrahedra (T = Si, Al) framework with the chemical formula $M^n_{x/n}Si_{1-x}Al_xO_2 \cdot yH_2O$ where M = e.g. Na^+, K^+, …. More than 238 distinct zeolite frameworks topologies have been recognized exhibiting stronger acidities and higher thermal/hydrothermal stabilities in comparison to several inorganic ion exchangers ([12]–2016). Thus, zeolites are in use in many industries and applications such as purification, adsorption, separation, and catalysis [11, 29, 52]. However, main disadvantages of ZT are: the high purification cost of natural ZT, tedious synthesis procedure, and the lack of versatility of its pore distribution as it possesses mostly micropores in its pure crystalline state (channels <0.8 nm and cavities <1.3 nm) ([10, 12]–2016; [33]). This deters the diffusion of large-sized ions such as cationic dyes [33].

Surfactant-templating (ST) has been confirmed to be one of the most adaptable and valuable techniques to implement ordered mesoporosity into frameworks of solid materials since reporting first material MCM-41 by Yanagisawa et al. [63]. Recently, a new technique was introduced combining the rewards of both MPS and zeolites using ST technique by partial isostructural replacement of Si^{4+} with Al^{3+} in a framework of MCM-41 either from alkoxysilanes [18, 60] or sodium silicate [4, 7] as silicon sources to synthesize ordered mesoporous Al-MCM-41. Sepehrian et al. [51], have reported a cheap "pH-adjusting" hydrothermal method to dope Al^{3+} ions into MCM-41. Al-MCM-41 was proved to acquire high cationic exchange capacities towards Methylene blue (MB) [18] and several metal ions such as Sr(II), Ce(III), U(VI) and Cd(II) [51]. Yue et al. [64] used aluminum tritert-butoxide and tetraethyl orthosilicate (TEOS) precursors to directly incorporate Al(III) into SBA-15 frame work [64]. Also, a different approach was introduced by Adjdir et al. [7] by applying volclay as a low-cost Si and Al source to produce Al-MCM-41 with a high surface area (>1000 m^2 g^{-1} and high mesoporosity (> 0.7 cm^3/g). However, the produced materials may lack homogeneity and the methods of synthesis incorporate expensive and toxic alkoxysilanes [18, 60].

Methylene blue (MB) is generally used as a basic dye in microbiology, medical diagnosis and treatment, ([24, 58] in addition to simple simulation of cationic dyes in adsorption studies. [40, 45, 70] In this paper, we report cost-effective synthesizing of a highly-stable MCM-41-like aluminosilicate cation exchanger with pure mesoporosity. The synthesized material was spectrally and analytically characterized, then the adsorption of MB as a model for a cationic dye using this ordered mesoporous material was studied and applied on different MB-contaminated water samples.

2 Experimental

2.1 Materials

All chemicals and reagents were of highest purity grade from Sigma–Aldrich otherwise stated. Sodium trisilicate (STS) $Na_2Si_3O_7$ (10% H_2O) and $AlCl_3$ were bought from Fluka, Switzerand. Cetyltrimethylammonium bromide (CTAB) was bought from Fluka (Germany). 0.001 mol L^{-1} stock solution of methylthioninium chloride (MB) ($C_{16}H_{18}N_3SCl\cdot3H_2O$ from Riedel-de Haën Co. (Germany)) was prepared by dissolving a calculated amount in DDW.

2.2 Equipment

The prepared samples were subjected to powder X-ray diffraction (XRD) analysis using Empyrean Powder Diffractometer equipped with a Cu K_α radiation and a Ni filter at constant voltage 40 kV, and 30 mA. Thermogravimetric analysis (TGA) was carried out on SDT Q600 (TA Instruments, USA) thermal analyzer under nitrogen using a heating rate of 10 °C min^{-1}. Scanning electron microscope (SEM) images were performed on JXA 840A electron probe microanalyzer, Japan attached with EDX Unit (Energy Dispersive X-ray Analyses), with accelerating voltage 30 K.V., magnification 14× up to 1,000,000. Fourier transform infrared (FTIR) spectra were recorded on a Nicolet iS10, Thermo-Fisher Scientific, USA, using KBr pellet. Specific surface area was calculated with a BELSORP-mini II, BEL Japan, INC, using nitrogen at 77 K. S_{BET} was calculated following the Brunauer, Emmett and Teller (BET) -method [8]; the degassing temperature was 300 °C. Electronic spectra were recorded on a UnicamUV/Vis UV2 for the supernatant solutions obtained after centrifuging suspensions. Estimation of residual MB was done by comparing their UV absorption at λ_{max} at 663.8 nm with calibration curve of MB solution (absorption at isobestic point 622 nm was measured to avoid absorption fluctuations due to MB aggregation and pH variation [21]. The pH of solution of each sample was adjusted with NaOH and H_2SO_4 solutions, using a Hanna Instruments, 8519, Italy, pH/mV meter with an expanded and ± 0.1 accuracy scale. Metrohm automatic potentiometer (848 Titrino) was exploited to perform the pH-metric titration. An amount of (100 mg) of the investigated sample was added to 25 mL of 0.5 mol L^{-1} KCl and titrated against 0.0073 mol L^{-1} KOH or 0.0086 mol L^{-1} HCl + 0.5 mol L^{-1} KCl at 17 °C with a titration rate of 0.1 mL min^{-1}.

2.3 Methods

Two different samples of mesoporous aluminosilicate were prepared using a modified method of Sepehrian et al. [51]. STS and anhydrous aluminum chloride ($AlCl_3$) were used as silicon and aluminum sources, respectively, in an atomic ratio

of Si/Al 13.64:1. In a typical procedure, 6 g of CTAB was poured in 100 mL of deionized water, then the mixture was kept under stirring for 15 min (400 rpm) till complete dissolution. Also, 34.52 g, (0.385 mol) of STS was boiled in 100 mL 23% aqueous solution of sodium hydroxide till complete dissolution, cooled to room temperature then poured into CTAB solution, further stirred for another 30 min, then DDW was added to adjust the volume to 230 mL. Another mixture containing 6 g of CTAB dissolved in 100 mL of deionized water, 3.77 g (0.028 mol) of anhydrous aluminum chloride dissolved in 100 mL of 6% sodium hydroxide solution (to form sodium aluminate solution) was stirred for 30 min, then DDW was added to adjust the volume to 230 mL. The two mixtures were mixed together and left under continuous stirring for 24 h at pH 9.2 ± 0.1. The obtained gel mixture was left to settle for another 24 h, filtered out, washed thoroughly with water, dried at 50 °C for 72 h and finally subjected to calcination at 500 °C for six hours. The product was named Al- MCM-41, For the purpose of comparison, the same procedures was followed without $AlCl_3$ addition to prepare MCM-41.

2.4 Adsorption Studies of Methylene Blue

The adsorption experiments were achieved at room temperature of 20 ± 1.0 °C and ambient initial pH of MB solutions 5.8, otherwise stated. The adsorption isotherm was studied by mixing 0.1 g of Al-MCM-41 with 50 mL of 10, 30, 50, 100, 200 and 300 mg L^{-1} initial concentrations of MB in a 100 mL stopper conical flasks under shaking for 30 min and then left for equilibration 24 h. Then the residual MB concentration was measured by UV-vis spectrometry.

The kinetics studies of MB-removal were carried out by vigorously stirring of 0.2 g of Al-MCM-41 with 100 mL of 100 mg L^{-1} of MB solutions; stirring was briefly interrupted at time intervals 5–90 min, while 1 mL volumes of supernatant solutions were pipetted out from the reactor, filtered out and analyzed to determine the residual MB concentration in the aqueous solution. After agitation for 90 min, the contents in the flask were filtered and the residual concentrations of MB were estimated using UV-vis spectrometry. The adsorption capacity (mg g^{-1}) at equilibrium (q_e) as well as at a given time t(q_t) were estimated out using the mass balance equations:

$$q_e = \frac{(C_0 - C_e)}{m} V \tag{1}$$

$$q_t = \frac{(C_0 - C_t)}{m} V \tag{2}$$

where C_0, C_e, and C_t refer to the liquid-phase concentrations (mg L^{-1}) of MB at start, equilibrium and time t, respectively; V is the volume of the solution (L) and m is the mass of adsorbent (g).

The effect of initial pH values on the adsorption behavior of MB was investigated by mixing 0.1 g of the adsorbent with 50 mL volume of 100 mg L^{-1} MB; Solutions of 0.1 $^{mol\ L^{-1}}$ NaOH and 0.1 HCl were used for adjusting the initial pH values of MB solutions (2.0–10.0). The resulting solutions containing adsorbent were agitated for 30 min, then were left overnight, filtered and the residual concentration of MB in solution was determined as described before.

For the effect of dosage studies, the initial pH value of 50 mL 100 mg L^{-1} MB was adjusted at 8.0 and shaken with 0.01–0.2 g Al-MCM-41 for 30 min. The concentration of the unadsorbed MB ions was determined after settlement of the adsorbent for an overnight.

The effect of solution salinity on MB uptake onto Al-MCM-41 was investigated in presence of NaCl, $MgSO_4$, and $CaCl_2$ in the range of concentration of 0.1–1.0 mol L^{-1}. The initial pH value of 50 mL 100 mg L^{-1} MB was adjusted at 8.0 and shaken with 0.1 g Al-MCM-41 for 30 min. The suspensions were left to settle overnight then the final concentration of the unadsorbed MB ions was determined as mentioned above. The decrease in removal efficiency (ΔE_r, %) was calculated according to Eq. (3):

$$\Delta E_r = 100 - \left(100 x \frac{q_e\ in\ presence\ of\ the\ salt}{q_e\ in\ absence\ of\ the\ salt} \right), \% \tag{3}$$

The regeneration study of the loaded Al-MCM-41 was performed on the adsorbent loaded at the conditions 50 mL of 100 mg L^{-1} MB, 0.1 g Al-MCM-41, initial pH 8.0, stirring time 30 min and overnight settling, then washed several times with distilled water, dried at 80 °C for 24 h and kept for analysis and desorption studies. The desorption processes were carried out on 0.02 g of the loaded MB-Al-MCM-41 shaken with 5 mL of 0.1 mol L^{-1} HCl, 7.5% sodium dodecylsulfate (SDS), acetone and ethyl alcohol for 1 h at 25 and/or 40 °C. The released dye concentration (C_r) was determined directly in the liqueurs after filtration except in case of acetone and ethanol where the solvents were first vaporized then the dye was dissolved in 5 mL. The desorption efficiency ($E\%$) was determined by the formula:

$$E = \frac{C_r}{C_{calc}} x 100\% \tag{4}$$

where C_{calc} (mg L^{-1}) is the loaded dye calculated from the q_t value.

The loaded sample was activated by heating at 400 °C in air after washing with water. Then the batch-mode capacity was examined using 0.1 g of the regenerated Al-MCM-41 and 100 μg mL^{-1} MB as initial concentration for a sample volume of 100 mL at pH 8.0 after time of shaking 30 min. Then the equilibrium capacity was determined as usual.

A batch-mode application of the adsorption of MB from natural water samples was applied after spiking with

100 mg L^{-1} MB. An amount of 0.1 g Al-MCM-41 was stirred in 50 mL of the water sample for 30 min at ambient pH and room temperature. Then the samples were filtered and residual MB concentration was determined.

3 Results and Discussion

3.1 Characterization of Al-MCM-41

The wide angle XRD pattern of Al-MCM-41 is shown in Fig. 1. It indicates the formation of an amorphous structure in the short-range packing of atoms, which is confirmed by the appearance of an amorphous hump at 2θ 23.9° typical to amorphous silica. Small angle region of XRD shows weak reflections at 2θ 2.47° ($2\theta_1$), 4.27° ($2\theta_2$) and 4.93° corresponding to d-spacing of 3.58, 2.07 and 1.79 nm, due to the d_{100}, d_{110} and d_{200} reflections, respectively, of a hexagonal ordered pore arrangement (P6mm space group) typical of MCM-41-like structure. The value of $\sin^2\theta_1/\sin^2\theta_2$ is equal to 0.33 which is very close to 1:3 ratio, suggesting a long-range ordered arrangement of pores [13].

No diffraction peak was observed in the region of $2\theta > 10°$ (Fig. 1), which indicates the absence of micro-crystals in the sample, suggesting that Al-MCM-41 is mostly X-ray amorphous. The length of the unit cell parameter (a_o) for the hexagonal pore system was calculated from the relation [57].

$$a_o = 2d_{100}/\sqrt[2]{3} \qquad (5)$$

The value of a_o was 4.13 nm which is slightly smaller than that reported for Al-MCM-41 (4.23 nm [51], 4.51 nm, [6]) which may be assigned to the difference of the synthesis parameters. This can be understood in view of the impact of MCM-41 synthesis parameters on the structure such as the
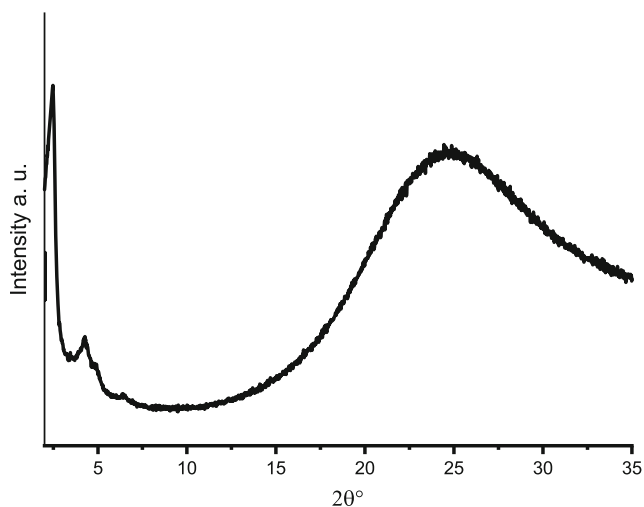
hydrogel composition, the type and length of the surfactant, the temperature, the alkalinity, and the synthesis time [39].

The N_2 adsorption-desorption isotherm of Al-MCM-41 exhibited type IV behavior with almost no hysteresis loop (Fig. 2a), typical for mesoporous MCM-41 materials with uniform porosity <4 nm [20]. This reversible adsorption desorption isotherms is a result of instability of the hemispherical meniscus throughout the desorption process in the pores triggered by an increased chemical potential of the pore walls, and accordingly an increased tensile strength in the adsorbed phase is observed as the pore size decreases [20]. Figure 2b demonstrated the formation of a mesoporous Al-MCM-41 structure with short close-packing range of SiO_4 tetrahedra and a uniform pore size distribution. The pore size distribution estimated from the adsorption branches of the isotherms using NLDFT model unveils the presence of uniform mesopores with an average pore diameter ($D_{p,NLDFT}$) of 2.73 nm. The BET surface area ($\alpha_{s,BET}$) and pore volume (V_p) dropped from 1020 m^2 g^{-1} and 0.86 mL g^{-1} for MCM-41 to 592 m^2 g^{-1} and
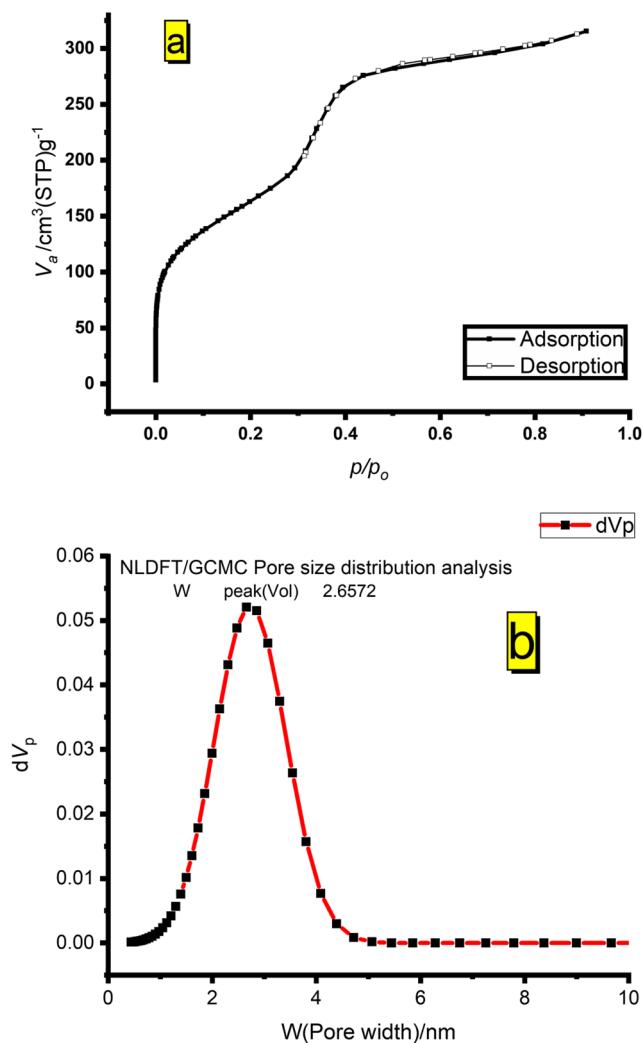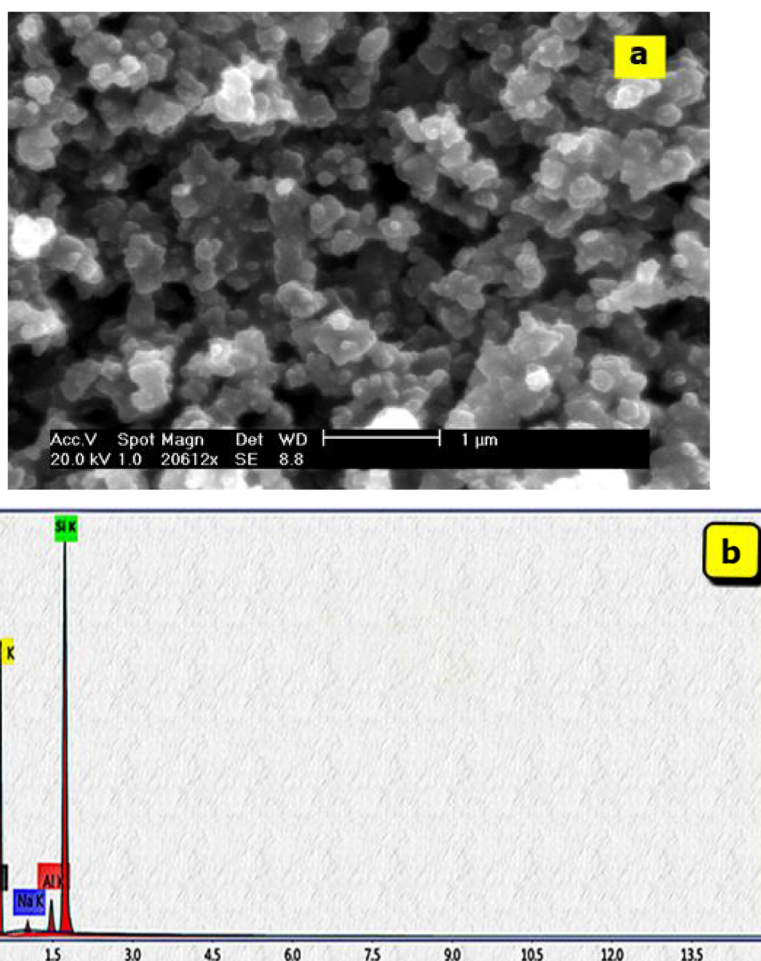

Fig. 2 (**a**) Nitrogen adsorption/desorption isotherm and (**b**) Pore size distributions of Al/MCM41.derived from N_2 adsorption

Fig. 1 XRD pattern of Al/MCM41

Parameters		Values								Unit
		Present study	[3]	[51]	[64]	[27]	[58]	[7]	[69]	
d_{100} from XRD		3.58	3.53	3.83	4.01	3.93	–	–	4.10	nm
α_o		4.13	4.08	4.23	4.63	4.54	4.75	4.53	4.44	nm
BET model	V_m	136.0	–	–	–	–	–	–	5.13	$cm^3(STP)\ g^{-1}$
	α_s	592	1020	792	847	1044	870	1060	1150	$m^2\ g^{-1}$
	$V_p\ (p/p_0 = 0.909)$	0.49	0.89	–	–	0.91	–	–	1.17	$cm^3\ g^{-1}$
	D_p	3.30	1.68	–	–	–	–	–	–	nm
NLDFT model	V_p	0.49	–	–	–	–	–	0.77	–	$cm^3\ g^{-1}$
	D_p	2.73	–	–	–	–	–	3.78	–	nm
Barrett–Joyner–Halenda (BJH) model*	D_p	–	–	2.44	2.5	3.86	3.14	–	–	nm
	V_p	–	–	0.73	1.01	0.68	0.51	–	–	$cm^3\ g^{-1}$
W_t		1.40	1.37	1.79	2.13	–	1.61	0.75	2.1	nm
Starting Si/Al atomic ratio		13.6/1	–	10/1	15/1	–	40.2/1	17/1	7–350/1	–
Found Si/Al atomic ratio		14.9	–	16.4/1	10/1	–	42.6/1	–	6–350/1	–
Reference		Present study	[3]	[51]	[64]	[27]	[58]	[7]	[69]	–

α_o: unit cell; as: BET specific surface area, V_p pore volume, D_p average pore diameter, W_t wall thickness

* BJH values are stated for the sake of comparison with older publications

0.50 mL g⁻¹, respectively for Al-MCM-41. Also, the pore diameter (D_p) slightly increases from 1.68 [3] to 2.73–3.30 nm. Reported $\alpha_{s,BET}$ and V_p values for Al-MCM-41 (792–1150 m² g⁻¹ 0.73–1.17 cm³ g⁻¹) are higher than that of the present study (592 m² g⁻¹ and 0.50 cm³ g⁻¹, respectively) whereas the D_p value of the present Al-MCM-41 (2.73–3.30 nm) is within the reported values (2.44–3.86 nm).

By combining XRD and surface area data, the wall thickness (W_t) can be calculated from the formula [28].

$$W_t = a_o - D_p \tag{6}$$

The W_t value of our synthesized Al-MCM-41 (1.40 nm) is less than that reported for similar composition (1.79 nm) [51]. Consequently, it is expected that the present Al-MCM-41 exhibits large α_s as observed for thin-walled materials shown in Table 1.

On contrary, the present material possessed low surface area that is attributed to its small α_o, and mesoporosity with small D_p and dense walls. Also, the important synthesis parameter in the present method is that both Al and Si sources are dissolved in NaOH solutions previous to the addition of CTAB which increases homogeneity of their resultant mixture (Al-MCM-41) as confirmed by SEM-EDX analysis (Fig. 3). SEM images of Al-MCM-41 revealed irregular spherical particles with a cross-linked network (Fig. 3a). EDX analysis was close to the expected Si/Al mole ratio (13.64:1.0) and the standard deviation of the elemental analysis was within 4.20–10.10 as illustrated in Table 2. EDX analysis (Fig. 3b) of Al-MCM-41showed that the atomic ratio of Si/Al is 14.9/1 which is close to that reported for alike structure (16.5/1.0) [51]. However, the Si/Al atomic ratio in the present study is remarkably closer to the starting ratio than that reported in the literature [51]. An obvious increase in Si/Al was usually observed [51, 62] possibly due to the preferable dissolution of Al(III) as aluminate in basic medium compared with Si(IV) [43]. Also, Na/Al mole ratio was 0.32 which is lesser than expected equimolar ratio indicating a partial replacement of Na⁺ with H⁺. However, high sodium content is not preferred as it was reported to catalyze hydrolysis ofMCM-41 silica and structure instability [46].

(Fig. 4a) depicted the pH-metric titration pattern of Al-MCM-41 against 0.0073 mol L⁻¹ KOH. The Al-MCM demonstrated a higher stability against hydrolysis comparing to MCM-41; this may be related to homogeneous inclusions of Al(III) into mesoporous silica framework. At the beginning of the titration curve, a shift of pH of approximately 3 units towards higher basic range was observed to occur for Al-MCM-41 compared with MCM-41 indicating the relative resistance to hydrolysis. Also, lesser KOH volume was consumed for Al-MCM-41 (6.54 mL) compared with MCM-41 (28.18 mL) at the same pH value (9.43) attributed to deprotonation of silanol (or aluminol) groups [1, 2]. A base

Fig. 3 a SEM **b** EDX analysis of Al/MCM41

catalyzed mechanism was previously suggested to elucidate the hydrolysis of silica. However, stabilization was achieved either by effective covering of silica surface [1]. or by doping with an electropositive element such as Zr(IV) [2]. The later method may be the case of the present Al-MCM-41 knowing that Al is more electropositive than Si.

Repeating the same titration against 0.0086 mol L^{-1} HCl (Fig. 4b), Al-MCM-41 shows almost the same response of the blank curve indicating the neutrality of the silica surface whilst on contrary, MCM-41 shows acidic nature as concluded from the small delay (0.36 mL) of the titration curve. Also, the starting pH of Al-MCM-41 was slightly shifted towards basic range (0.36) compared with the blank whereas MCM-41 starting pH was strongly boosted downwards with a shift of 1.19.

Table 2 EDX analysis of Al/MCM41

Element	Concentration, mass%	Concentration, X/Al mole ratio
Na	0.94 ± 0.095	0.32
Al	3.47 ± 0.20	1.0
Si	53.77 ± 2.27	14.9

Furthermore, the total concentration of consumed protons in the titration process (Q_H, mol g^{-1}) is calculated from Eq. (7) [61]:

$$Q_H = \frac{C_A - C_B + [OH^-] - [H^+]}{C_s} \qquad (7)$$

where C_A and C_B are the concentration (mol L^{-1}) of HCl and KOH respectively, [H$^+$] and [OH$^-$] are the concentration of H+ and OH−, Cs is the concentration of sorbent in the suspension (g L^{-1}). Figure 5 shows the variation in Q_H values of MCM-41 and Al-MCM-41 versus pH. Two distinct deprotonation stages could be distinguished for both samples although the stages are shifted to higher pH in Al-MCM-41. These stages were reported previously for a Al-MCM-41-like phase developed from montmorillonite with acidity constants of ≡Al/SiOH sites (pKa) of 3.2 and 4.9. They were attributed to the deprotonation of ≡Al/SiOH$_2^+$ (≡Al/SiOH$_2^+$↔ ≡ Al/SiOH + H$^+$) and ≡Al/SiOH (≡Al/SiOH↔ ≡ Al/SiO$^-$ + H$^+$), respectively [17].

The Acid–base titration curve showed that the of zero-point charge pH values (pH$_{zpc}$) of MCM-41 and Al-MCM-41 are 4.1 and 6.0, respectively. The reported pH$_{zpc}$ values for alike
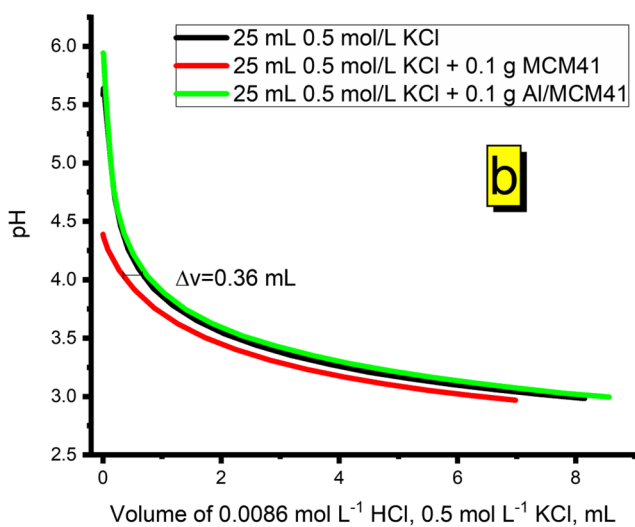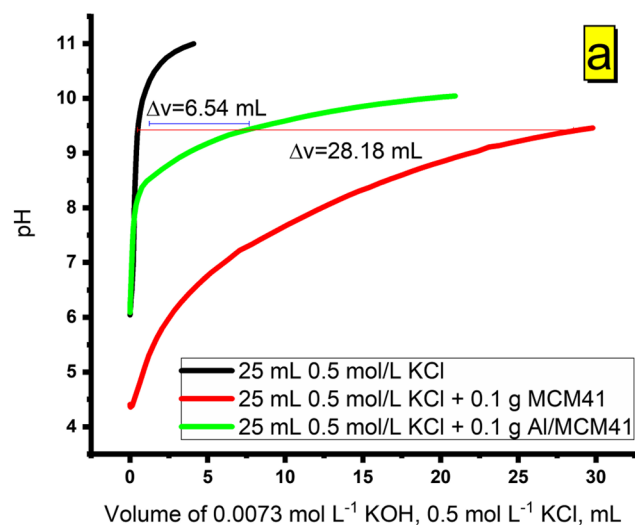
Fig. 4 pH metric titration of Al/MCM41 and MCM41 0.0073 mol L^{-1} KOH, 0.5 mol L^{-1} KCl, mL (**a**) against Volume of 0.0086 mol L^{-1} HCl, 0.5 mol L^{-1} KCl, mL (**b**)
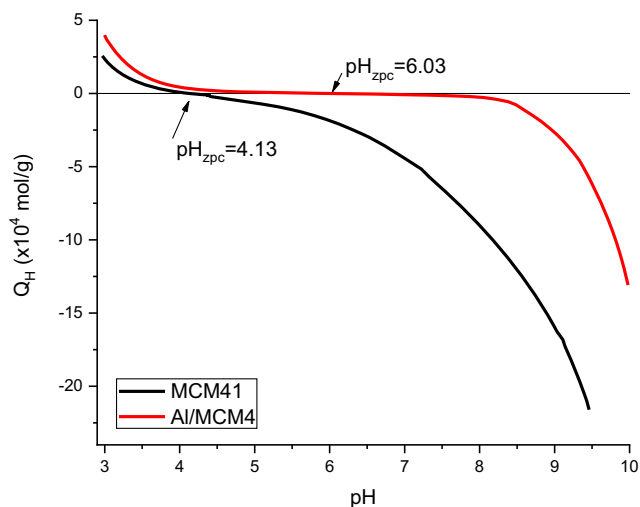
Fig. 5 Acid–base titration of 100 mg of MCM41 (black) and Al/MCM41 (red) in 0.5 mol L^{-1} KCl at T = 25 °C

Al-MCM-41 are in the 4.1–4.4 range, which are close to that of MCM-41 but much lesser than the present Al-MCM-41. This provides another sign to relatively better enhancement in the stability of Al-MCM-41 due to well inclusion of Al^{3+} ions in the silica matrix.

The FT-IR spectra of Al-MCM-41 shown in Fig. 6 is typical to vibrations of similar structures [51]. Al-MCM-41 exhibited absorption bands at approximately 3452 cm^{-1} assigned to the stretching vibrations of OH units of adsorbed water and hydrogen-bonded silanol groups. The absorption band around 1625 cm^{-1} is assigned to deformed vibration of adsorbed water. The observed absorption band at 1080 cm^{-1}, accompanied by a shoulder at 1221 cm^{-1} and the band located at 796 cm^{-1}, are assigned to internal and external asymmetric Si-O stretching modes respectively. The shoulder in region 950–970 cm^{-1} was generally considered as a proof for the incorporation of Al(III) into the framework [51]. The bands at 459, 539 and 695 cm^{-1} may be assigned to symmetrical stretch (n_{sym}), external linkage vibration of five-membered rings of T-O-T order and asymmetrical stretch (n_{asym}), respectively [19].

The TGA of Al-MCM-41 (Fig. 7) shows two stages of mass loss up to 750 °C, which is typical to alike structures [51]. The stages can be distinguished as 35–150 and 150–550 °C. The mass loss in the first stage is 14.7% and is due to desorption of physisorbed water held in the pores. The mass loss during the second stage (3.5%) is mainly due to the condensation of silanol groups.

3.2 Adsorption Study of MB on Al-MCM-41

3.2.1 Effect of Initial MB Concentration

Figure 8 shows the effect of initial MB concentration on its adsorption onto Al-MCM-41. It was observed that q_e increased with increasing MB concentration from 10 to 300 mg L^{-1}.
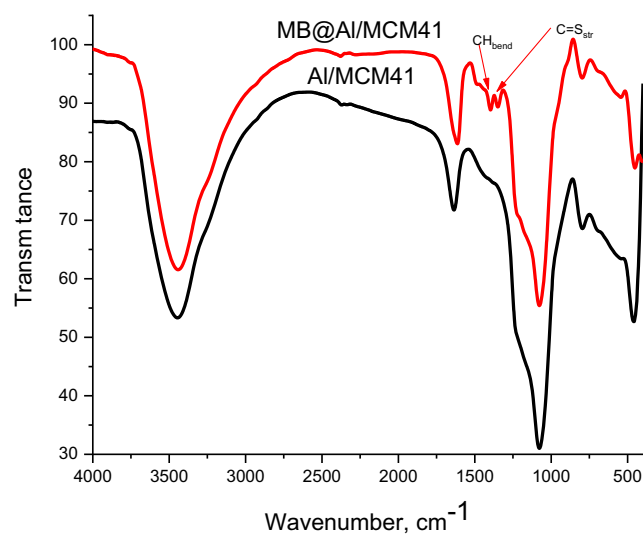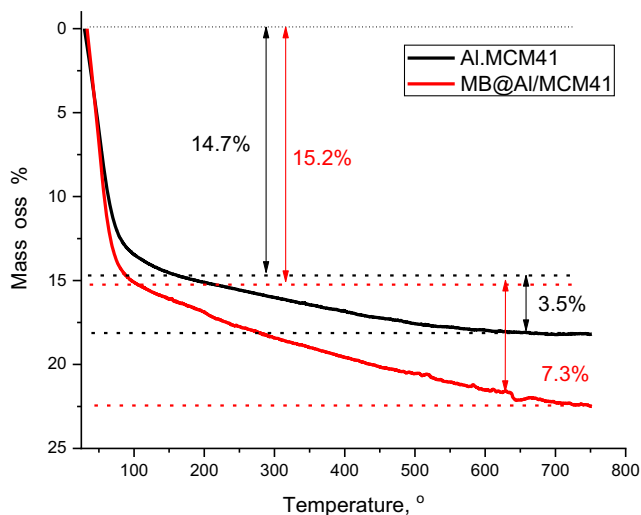
Fig. 7 TGA of Al/MCM41 and MB@Al/MCM41

Isotherms models were studied for characterizing the adsorption process such as Langmuir and Freundlich isotherms, which provide information on the capacity of sorbent. These isotherms demonstrate a reliant of the dye uptake per unit mass (q_e) on the equilibrium metal ion concentration (C_e) (Fig. 8).

Langmuir isotherm model proposes that the adsorption uptake takes place on a homogeneous surface by a monolayer sorption neglecting the adsorbent molecules interactions [32]. It adopts uniform adsorption energies on the surface and no adsorbate transmigration. From Table 3, K_L value for MB ion adsorption was found to be 0.11 L g^{-1} that is less than 1, suggesting that the Al-MCM-41 adsorbent are highly favorable for the adsorption of MB ions from aqueous solution.

Accordingly, the maximum adsorption capacity evaluated from Langmuir model (q_m) was found to be 285 mg g^{-1} for adsorption of MB ions on Al-MCM-41, indicating the effectiveness of the synthesis method in creating good sorption sites. In addition, the fitness of linear form evaluated from two models was examined by estimation of the linearity or regression coefficients (R^2). Langmuir model isotherm (not shown here **SI**) was found to define the adsorption of MB ions
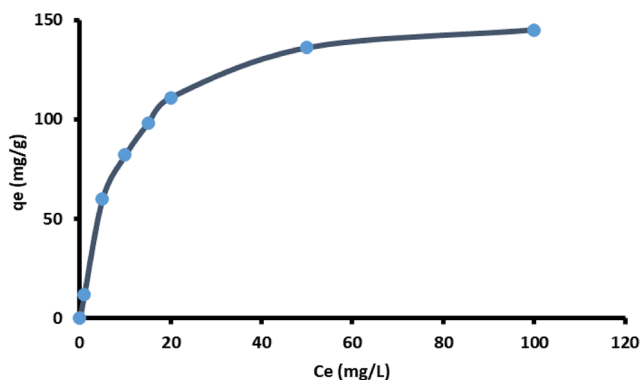
Fig. 8 Effect of initial MB concentration on its adsorption onto Al/MCM41(the initial concentration ranged from (10 300 mg L^{-1})

Table 3 Langmuir and Freundlich, D R for MB sorption onto Al/MCM41 at 303 K

Models	Isotherm parameters		
	q_m (mg/g)	K_L (L/g)	R^2
Langmuir	285.0	0.1118	0.9717
	K_F	n	R^2
Freundlich	5.738	0.1706	0.5693

on Al-MCM-41 better than Freundlich isotherm (not shown here **SII**) because its R^2 value was (0.97) that is remarkably higher that obtained from Freundlich (0.56). The obtained monolayer capacity (285 mg g^{-1} ≡ 0.89 mmol g^{-1}) is lower than that of the theoretical cationic ion exchange capacity, concluded from Al% (1.29 mmol g^{-1}), which may indicate that almost 31% of active sites attributed to Al content are inaccessible to the bulky MB ions. However, the MB capacity was observably higher than those reported for some alumino silicates such as Al-MCM-41 (66.5 mg g^{-1}) [18] kaolin (30 mg g^{-1}) [49] and zeolites (33.5–38.4 mg g^{-1}) ([49, 56] (Table 4). This may be related to the confirmed homogeneous distribution of Al(III) in the silica framework attained according to the present study. Also, the monolayer MB capacity of Al-MCM-41 is also higher than those obtained for activated carbon and *Citrus limetta* peel (8.76–250 mg g^{-1}) [9] [36, 54].

3.2.2 Effect of Time of Shaking

The effect of time of shaking on the adsorption of MB by Al-MCM-41 was investigated from 2.0 to 45 min shaking time (Fig. 9). It was observed that the MB removal percentage by Al-MCM-41 increased with increasing time of shaking and reached stability of removal efficiency of 93.2% of C_i (100 mg L^{-1}) at 30 min. This equilibration time is better than the reported results (50 min) for alike Al-MCM-41 [18] and some recently reported adsorbents [19, 56], [9] as detailed in Table 4.

Adsorption kinetic studies of MB onto Al-MCM-41 were examined by the pseudo–first order, pseudo–second order and intraparticle diffusion models, described previously [16]. The characteristic parameters are given in Table 5 showing that the adsorption of MB ions on treated Al-MCM-41 is best described by pseudo-second order kinetic model with a high correlation coefficient (0.988). This supposes that the heterogeneous sorption mechanism is likely to be responsible for the uptake of MB ions onto Al-MCM-41.

3.2.3 Effect of pH

The influence of variation of initial pH values (2.0–10.5) on the amount of adsorbed MB ions onto Al-MCM-41 was studied at equilibration time of 60 min as shown in Fig. 10. It is
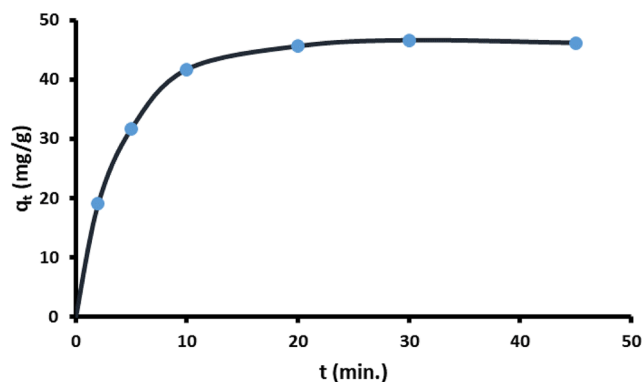
Table 4 Comparison between the adsorption parameters of the present Al/MCM41 adsorbent for MB with recently reported adsorbents

Adsorbent	Removal efficiency (%)	Capacity (mg g^{-1})	C_i(mgL^{-1})/v(mL)/dosage (g L^{-1})	Equilibration time (min)	pH	pH
Al/MCM41	98.7	285	100/100/1.0	30	8	This work
Al/MCM41	94.0	66.5	3.20/200/0.025	~50	7	[20]
MCM41	54.0	10.95	25	12	7	[65]
MCM41	44.0	73.5	30	15	7	[68]
Silica nanosheet		11.77	28.79	90	7	[71]
Silica gel	62.0	23.3	200	90		[59]
SBA 15	100	280	30/100/0.25	5	8 12	[17]
Citrus limetta peel	97.1	227.3	50/25/2	30	4 10	[54]
Activated carbon web	90.0	8.76	6.0/50.0/3.0	125	2, 11	[43]
Activated carbon		250		60	8 12	[34]
starch g poly(acrylic acid)		1532		30	6 9	[37]
Kaolin	93.8	30.0	7.5/ /0.5	40	4	[50]
Zeolite 4A	95.7	33.5	7.5/ /1.0	40	5	[50]
Nano Mordenite zeolite		38.4	3.2/200/0.25	150	9	[57]

clear that the equilibrium adsorption capacity of the adsorbent (q_e, mg g^{-1}) towards MB increases as the pH increases and reached maximum adsorption at pH 8.0 at which the adsorbent is fairly stable as concluded above (Fig. 4a and 5). This pH value for maximum MB adsorption (8.0) is optimal for natural water treatment as its pH mostly ranges from 7.0 to 8.5 that gives advantage for the present adsorbent in comparison with many reported materials that requires pH control beyond its ambient values (Table 4).
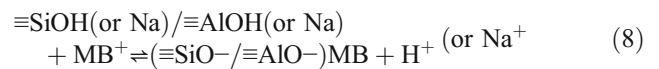
The relatively low uptake of MB in acidic medium has been also reported elsewhere for various adsorbents and was attributed to the competition of MB$^+$ with H$^+$ [15, 18]. This may be attributed to the weak acidic nature of the surface of Al-MCM-41 confirmed above (Fig. 5). The increase of MB adsorption with increasing pH was attributed to the deprotonation of surface -OH groups on the adsorbent [18] which is supported from pH-metric titration study. A slight decrease in adsorption of MB on Al-MCM-41 at pH > 8.0 was observed

that may be due to the silica hydrolysis known to occur in alkaline media [1]. The electrostatic repulsion between the negatively charged surface and the Zwitter ion of MB was suggested to occur at high pH value [18] but this explanation was rejected as the claimed structure of MB is wrong.

Consequently, the adsorption of MB onto Al-MCM-41 may be expressed according to the equation:

$$\equiv\text{SiOH(or Na)}/\equiv\text{AlOH(or Na)} + \text{MB}^+ \rightleftharpoons (\equiv\text{SiO}-/\equiv\text{AlO}-)\text{MB} + \text{H}^+ \text{ (or Na}^+) \quad (8)$$

3.2.4 Effect of Al-MCM-41 Dosage

The variation of the removal efficiency of Al-MCM-41, using various dosages of 0.01 to 0.10 g for 100 mg L^{-1} MB was also

Fig. 9 Effect of shaking time on the adsorption of MB (initial concentration 100 mg L^{-1}) onto 0.1 g Al/MCM41

Table 5 Kinetic parameters for the MB adsorption onto Al/MCM41

Pseudo first order constant

k_1(g mg^{-1} min^{-1})	q_e (mg g^{-1})	R^2
0.057	16.71	0.855

Pseudo second order constant

k_2(g mg^{-1} min^{-1})	q_e (mg g^{-1})	R^2
0.065	71.43	0.988

Intra Particle diffusion Constants

k_{id}	C	R^2
12.97	1.42	0.989

k_1 is the adsorption rate constant (min^{-1}). k_2 (g/mg. min) is the rate constant of second order adsorption. k_{ipd} is the intraparticle diffusion rate constant (mg/g.min$^{1/2}$)
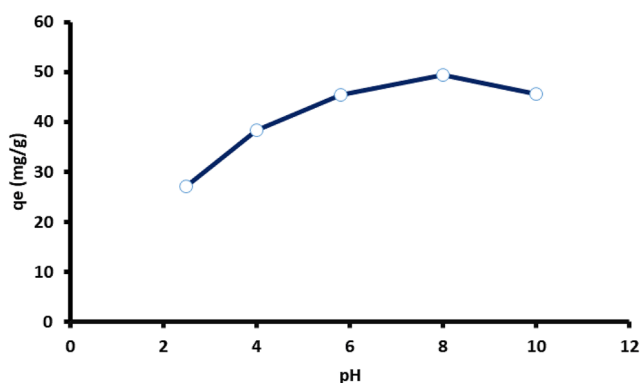
Fig. 10 Effect of initial pH on the MB adsorption onto Al/MCM41

studied (**SIII**). Increasing the dosage of adsorbent over this range resulted in an increase in the removal efficiency up to 97.5%. This dosage percentage is moderate compared with other adsorbents as shown in (Table 4) nevertheless the present Al-MCM-41 is characterized by cost-effective and eco-friendly material.

3.2.5 Effect of Salinity on the Uptake of MB on Al-MCM-41

As salinity is an important water quality parameter upon which the properties and the type of the water depends, the effect of the type of the salt and its concentration on the MB uptake onto Al-MCM-41 was studied as shown in Table 6. The removal efficiency of Al-MCM-41 towards MB was observed to decrease in the order NaCl > CaCl$_2$ > MgSO$_4$. In respect to the cation exchange characteristics of Al-MCM-41 confirmed from the adsorption studies, this trend may be correlated with the ionic radii of the cations which decrease in the same trend; 90, 86 and 59, respectively. In addition, MB removal efficiency onto Al-MCM-41 was observed to decrease with the increase in salinity. This behavior was observed previously for the adsorption extent of MB on kaolin and zeolite which was explained as the presence of salt ions in the solution screens the electrostatic interaction between the oppositely charged oxide surface and dye molecules, which results in diminishing the adsorbed amount as the salinity increases [49]. Also, a slow competition of the ions of the salt of the solution and the other cations forming the aluminosilicate was suggested to take place. On the other hand, solution ionic strength may affect the electrical double layer leading to a decrease in its thickness, hereby results in a decrease in adsorption.

3.2.6 Sorbent Regeneration

The regeneration of sorbent efficiency is an economic and environment-concern issue as far as secondary-waste is not recommended. SDS was the most effective releaser of MB (20% of the initial concentration), then 0.1 mol L^{-1} HCl (2.1%) whilst ethanol and acetone did not exceed 1% release despite heating up to 40. Accordingly, calcination of MB-Al-MCM-41 at 400 °C for one h was examined after primary washing and drying at 80 °C. Then, the adsorption process of MB was repeated at optimum conditions. A removal efficiency of 98% for MB onto Al-MCM-41 which is very comparable to the as synthesized efficiency.

3.3 Loading MB on Al-MCM-41

IR absorption study of MB@Al-MCM-41 shows the development of new bands at 1403 and 1350 cm^{-1} compared with that of Al-MCM-41 which are attributed to C-H bending [44] and the heterocycle C = S$^+$ stretching [48] vibration modes of MB and consequently indicate the successful loading of MB. Also, TGA curve of MB@Al-MCM-41 confirms the same idea as it shows an additional gradual increase in the mass loss (3.8%) within the heating range 200–500 °C compared with that of Al-MCM-41 which is attributable to the thermal degradation of the loaded MB.

3.4 Application Process

Batch-mode separation of 100 mg L^{-1} MB (spiked into the water samples) onto Al-MCM-41 was investigated on Nile river and Alkhadraweya canal waters from Dakahlia governorate at ambient pH values (7.0). The MB removal efficiencies were appreciably high (94.7 and 92.0%, respectively). These results indicate the feasibility of the removal process for cationic dyes from contaminated aqueous samples.

4 Conclusion

The synthesis of a homogeneous Al-MCM-41 cation exchanger was successfully accomplished due to modification of the reported process by introducing Al^{3+} to the reaction pot as aluminate ions (instead of Al(NO$_3$)$_3$.6H$_2$O). XRD and

Table 6 Effect of type of salt and its concentration on the MB uptake onto Al/MCM41	Salt	Concentration of salt (mol L^{-1})	q_e (mg g)	Decrease in removal efficiency (%)
		0.0	45.1	0.0
	NaCl	0.1	34.4	23.8
		1.0	31.0	31.3
	MgSO$_4$	0.1	43.0	4.8
	CaCl$_2$	0.1	35.0	22.5

surface investigations confirmed that the present material possessed thin W_t value (1.39 nm), the lowest surface area ($\alpha_{s,BET}$ = 592 m^2 g^{-1}), that was explained by acquiring narrowest ever reported α_o (4.13 nm), pure mesopores of small D_p (2.73 nm) and dense walls with negligible micropores. This resulted in stability enhancement of Al-MCM-41 against hydrolysis as evidenced from the upward shift of pH$_{zpc}$ (6.0) compared with MCM-41 and reported Al-MCM-41 (4.4). Also, the adsorption parameters become more appropriate for efficient adsorption of MB onto Al-MCM-41 at ambient conditions of natural waters. Optimum pH was 8.0, time of equilibration 30 min, C_i(mg L^{-1})/v(mL)/dosage (g L^{-1}) 100/100/1, capacity of 285 mg MB per g of adsorbent and removal efficiency 98.5%. This is assigned to the deprotonation of the surface edge-OHs.

Also, the adsorption process fitted the pseudo-second-order model which indicates that the rate is limited by intraparticle diffusion process. The Langmuir models could describe the equilibrium isotherms well.

Loaded Al-MCM-41 was confirmed to be easily and efficiently regenerated. It was successfully applied for the treatment of natural water samples spiked with MB.

Compliance with Ethical Standards

Conflict of Interest The authors declare that they have no conflict of interest.

References

1. Abou El Sherbini KS, Schiel D, Stosch R, Weidler P, Höll WH (2011) Stabilization of quercetin functionalized silica gel against hydrolysis by blocking silanol groups with TiO2 or ZrO2 and its application for the removal of hg (II). J Sol Gel Sci Technol 57:57 67

2. Abou El Sherbini KS, Weidler PG, Schiel D, Amr MH, Niemann H, El Dafrawy S, Höll WH (2014) Stabilization of silica gel against hydrolysis by doping with F or Zr (IV). Green and Sustainable Chemistry 4(24):32

3. Abou El Sherbini KS, Amer MH, Abdel Aziz MS, Hamzawy EM, Sharmoukh W, Elnagar MM (2018) Encapsulation of Biosynthesized Nano Silver in Silica Composites for Sustainable Antimicrobial Functionality. Global Challenges 2(8). https://doi.org/10.1002/gch2.201800048

4. Abou El Sherbini KS, Amr MHA, Abdel Aziz MS, Hamzawy EMA, Sharmoukh W, Elnagar MM (2019) under publication.

5. Adam J et al (2005) Pyrolysis of biomass in the presence of Al MCM 41 type catalysts. Fuel 84:1494 1502

6. Adeyemo AA, Adeoye IO, Bello OS (2017) Adsorption of dyes using different types of clay: a review. Appl Water Sci 7:543 568. https://doi.org/10.1007/s13201 015 0322 y

7. Adjdir M, Ali Dahmane T, Friedrich F, Scherer T, Weidler P (2009) The synthesis of Al MCM 41 from volclay a low cost Al and Si source. Appl Clay Sci 46:185 189

8. American Society of Health System Pharmacists, AHFS Drug Information. 2008, Bethesda, Md.: American Society of Health System Pharmacists,: Bethesda, Maryland pp. 1840.

9. Borade RB, Clearfield A (1995) Synthesis of aluminum rich MCM 41. Catal Lett 31:267 272. https://doi.org/10.1007/bf00808839

10. Brunauer S, Emmett PH, Teller E (1938) Adsorption of gases in multi molecular layers. J Am Chem Soc 60:309 319

11. Cashin VB, Eldridge DS, Yu A, Zhao D (2018) Surface functionalization and manipulation of mesoporous silica adsorbents for improved removal of pollutants: a review environmental science: Water Research & Technology

12. Cejka J, Van Bekkum H, Corma A, Schueth F (2007) Introduction to zeolite molecular sieves vol 168. Elsevier

13. Cheng Z L, Y x L, Liu Z (2018) Study on adsorption of rhodamine B onto Beta zeolites by tuning SiO 2/Al 2 O 3 ratio. Ecotoxicol Environ Saf 148:585 592

14. Christian Baerlocher LM, Wei Wan, Xiaodong Zou, Christine Kirschhock, Eric Breynaert, Anton Kirschhock, Vladislav Blatov, Olga Blatova, Mike Treacy (1996 2016) The Database of Zeolite Structures

15. Dang W, Han S, Xu J, Yan X, Hou W (2004) Effect of formamide on the morphologies of ordered mesoporous silica. Chinese J Inorg Chem 20:679 682

16. Doke SM, Yadav GD (2014) Novelties of combustion synthesized titania ultrafiltration membrane in efficient removal of methylene blue dye from aqueous effluent. Chemosphere 117:760 765

17. Dong Y, Lu B, Zang S, Zhao J, Wang X, Cai Q (2011) Removal of methylene blue from coloured effluents by adsorption onto SBA 15. J Chem Technol Biotechnol 86:616 619

18. Drweesh SA, Fathy NA, Wahba MA, Hanna AA, Akarish AIM, Elzahany EAM, El Sherif IY, Abou El Sherbini KS (2016) Equilibrium, kinetic and thermodynamic studies of Pb (II) adsorption from aqueous solutions on HCl treated Egyptian kaolin. J Environ Chem Eng 4:1674 1684

19. Du E, Yu S, Zuo L, Zhang J, Huang X, Wang Y (2011) Pb (II) sorption on molecular sieve analogues of MCM 41 synthesized from kaolinite and montmorillonite. Appl Clay Sci 51:94 101

20. Eftekhari S, Habibi Yangjeh A, Sohrabnezhad S (2010) Application of AlMCM 41 for competitive adsorption of methy lene blue and rhodamine B: thermodynamic and kinetic studies. J Hazard Mater 178:349 355

21. Flanigen E, Khatami H, Seymenski H, Flanigen E, Sand L (1971) Adv. Chemistry series 101 American Chemical Society, Washington, DC:201 228

22. Groen JC, Peffer LA, Pérez Ramírez J (2003) Pore size determination in modified micro and mesoporous materials. Pitfalls and limitations in gas adsorption data analysis. Microporous Mesoporous Mater 60:1 17

23. Hassanien MM, Abou El Sherbini KS, Al Muaikel NS (2010) Immobilization ofmethylene blue onto bentonite and its application in the extraction of mercury (II). J Hazard Mater 178:94 100

24. Henze M, Harremoes P, la Cour Jansen J, Arvin E (2001) Wastewater treatment: biological and chemical processes. Springer Science & Business Media

25. Hernandez Martínez A et al (2018) Swelling and methylene blue adsorption of poly (N, N dimethylacrylamide co 2 hydroxyethyl methacrylate) hydrogel. React Funct Polym 122:75 84

26. Hosseinian L, Weiner M, Levin MA, Fischer GW (2016) Methylene blue: magic bullet for vasoplegia? Anesth Analg 122: 194 201

27. Huo C, Ouyang J, Yang H (2014) CuO nanoparticles encapsulated inside Al MCM 41 mesoporous materials via direct synthetic route. Sci Rep 4:3682

28. Jorfi S, Barzegar G, Ahmadi M, Soltani RDC, Takdastan A, Saeedi R, Abtahi M (2016) Enhanced coagulation photocatalytic treatment of acid red 73 dye and real textile wastewater using UVA/synthesized MgO nanoparticles. J Environ Manag 177:111 118

29. Khanday WA, Marrakchi F, Asif M, Hameed BH (2019) Mesoporous zeolite activated carbon composite from oil palm ash as an effective adsorbent for methylene blue. J Taiwan Inst Chem Eng. https://doi.org/10.1016/j.jtice.2016.10.029

30. Kruk M, Jaroniec M, Sakamoto Y, Terasaki O, Ryoo R, Ko CH (2000) Determination of pore size and pore wall structure of MCM 41 by using nitrogen adsorption, transmission electron microscopy, and X ray diffraction. J Phys Chem B 104:292 301

31. Kulprathipanja S (2010) Zeolites in industrial separation and catalysis. Wiley Online Library, Kumari S, Chauhan GS, Ahn JH (2016) Novel cellulose nanowhiskers based polyurethane foam for rapid and persistent removal of methylene blue from its aqueous solutions. Chem Eng J 304:728 736. https://doi.org/10.1016/j.cej.2016.07.008

32. Kurade MB, Waghmode TR, Patil SM, Jeon B H, Govindwar SP (2017) Monitoring the gradual biodegradation of dyes in a simulated textile effluent and development of a novel triple layered fixed bed reactor using a bacterium yeast consortium. Chem Eng J 307:1026 1036. https://doi.org/10.1016/j.cej.2016.09.028

33. Langmuir I (1918) The adsorption of gases on plane surfaces of glass, mica and platinum. J Am Chem Soc 40:1361 1403. https://doi.org/10.1021/ja02242a004

34. Li Y, Yu J (2014) New stories of zeolite structures: their descriptions, determinations, predictions, and evaluations. Chem Rev 114:7268 7316

35. Li Z, Chang P H, Jiang W T, Jean J S, Hong H (2011) Mechanism of methylene blue removal from water by swelling clays. Chem Eng J 168:1193 1200. https://doi.org/10.1016/j.cej.2011.02.009

36. Li D, Yan J, Liu Z (2016) Adsorption kinetic studies for removal of methylene blue using activated carbon prepared from sugar beet pulp. Int J Environ Sci Technol 13:1815 1822

37. Liu X, Wei Q (2016) Removal of methylene blue from aqueous solution using porous starch g poly (acrylic acid) super adsorbents. RSC Adv 6:79853 79858

38. Liu B, Chen X, Zheng H, Wang Y, Sun Y, Zhao C, Zhang S (2018) Rapid and efficient removal of heavy metal and cationic dye by carboxylate rich magnetic chitosan flocculants: role of ionic groups. Carbohydr Polym 181:327 336

39. Malamis S, Katsou E (2013) A review on zinc and nickel adsorption on natural and modified zeolite, bentonite and vermiculite:examination of process parameters, kinetics and isotherms. J Hazard Mater 252:428 461

40. Meynen V, Cool P, Vansant E (2009) Verified syntheses of mesoporous materials. Microporous Mesoporous Mater 125:170 223

41. Mohammed M, Shitu A, Ibrahim A (2014) Removal of methylene blue using low cost adsorbent: a review. Research Journal of Chemical Sciences ISSN 2231:606X

42. Mouni L et al (2018) Removal of methylene blue from aqueous solutions by adsorption on kaolin: kinetic and equilibrium studies. Appl Clay Sci 153:38 45

43. Naeem S, Baheti V, Wiener J, Marek J (2016) Removal of methylene blue from aqueous media using activated carbon web. J Text Inst:1 9

44. North MR, Fleischer MA, Swaddle TW (2001) Precipitation from alkaline aqueous aluminosilicate solutions. Can J Chem 79:75 79

45. Ovchinnikov OV, Smirnov MS, Shatskikh TS, Khokhlov VY, Shapiro BI, Vitukhnovsky AG, Ambrozevich SA (2014) Spectroscopic investigation of colloidal CdS quantum dots methylene blue hybrid associates. J Nanopart Res 16:2286

46. Pathania D, Sharma S, Singh P (2017) Removal of methylene blue by adsorption onto activated carbon developed from Ficus carica bast. Arab J Chem 10:S1445 S1451

47. Pauly TR, Petkov V, Liu Y, Billinge SJ, Pinnavaia TJ (2002) Role of framework sodium versus local framework structure in determining the hydrothermal stability of MCM 41 mesostructures. J Am Chem Soc 124:97 103

48. Pharmacists ASoHS (2008) AHFS drug information 2008. Bethesda

49. Rao C, Venkataraghavan R, Kasturi T (1964) Contribution to the infrared spectra of organosulphur compounds. Can J Chem 42:36 42

50. Rida K, Bouraoui S, Hadnine S (2013) Adsorption of methylene blue from aqueous solution by kaolin and zeolite. Appl Clay Sci 83:99 105

51. Salem MA, Elsharkawy RG, Hablas MF (2016) Adsorption of brilliant green dye by polyaniline/silver nanocomposite: kinetic, equilibrium, and thermodynamic studies. Eur Polym J 75:577 590

52. Sepehrian H, Ahmadi S, Waqif Husain S, Faghihian H, Alighanbari H (2010) Adsorption studies of heavy metal ions on mesoporous aluminosilicate, novel cation exchanger. J Hazard Mater 176:252 256

53. Serrano DP, Melero JA, Morales G, Iglesias J, Pizarro P (2018) Progress in the design of zeolite catalysts for biomass conversion into biofuels and bio based chemicals. Catal Rev 60:1 70

54. Shahbazi A, Younesi H, Badiei A (2013) Batch and fixed bed column adsorption of Cu (II), Pb (II) and Cd (II) from aqueous solution onto functionalised SBA 15 mesoporous silica. Can J Chem Eng 91:739 750

55. Shakoor S, Nasar A (2016) Removal of methylene blue dye from artificially contaminated water using Citrus limetta peel waste as a very low cost adsorbent. J Taiwan Inst Chem Eng 66:154 163. https://doi.org/10.1016/j.jtice.2016.06.009

56. Soares PA, Batalha M, Souza SMGU, Boaventura RA, Vilar VJ (2015) Enhancement of a solar photo Fenton reaction with ferric organic ligands for the treatment of acrylic textile dyeing wastewater. J Environ Manag 152:120 131

57. Sohrabnezhad S, Pourahmad A (2010) Comparison absorption of new methylene blue dye in zeolite and nanocrystal zeolite. Desalination 256:84 89

58. Souza MJ, Araujo AS, Pedrosa AM, Marinkovic BA, Jardim PM, Morgado E (2006) Textural features of highly ordered Al MCM 41 molecular sieve studied by X ray diffraction, nitrogen adsorption and transmission electron microscopy. Mater Lett 60:2682 2685

59. Sulistiyo YA et al (2017) Silica gels from coal fly ash as methylene blue adsorbent: isotherm and kinetic studies. Bulletin of Chemical Reaction Engineering & Catalysis 12(2):263 272

60. Tardivo JP et al (2005) Methylene blue in photodynamic therapy: from basic mechanisms to clinical applications. Photodiagn Photodyn Ther 2:175 191

61. Tran HN, Van Viet P, Chao H P (2018) Surfactant modified zeolite as amphiphilic and dual electronic adsorbent for removal of cationic and oxyanionic metal ions and organic compounds. Ecotoxicol Environ Saf 147:55 63

62. Wang Z, Ling H, Shi J, Stampfl C, Yu A, Hunger M, Huang J (2018) Acidity enhanced [Al] MCM 41 via ultrasonic irradiation for the Beckmann rearrangement of cyclohexanone oxime to ε caprolactam. J Catal 358:71 79

63. Wei J, Wu D, Diao G, Peng J (2000) Modeling of lead adsorption on kaolinite. Diqiu Huaxue 29:397 401

64. Wu S, Li F, Xu R, Wei S, Li G (2010) Synthesis of thiol functionalized MCM 41 mesoporous silicas and its application in Cu (II), Pb (II), Ag (I), and Cr (III) removal. J Nanopart Res 12:2111 2124

65. Xiao X, Zhang F, Feng Z, Deng S, Wang Y (2015) Adsorptive removal and kinetics of methylene blue from aqueous solution using NiO/MCM 41 composite. Physica E: Low dimensional Systems and Nanostructures 65:4 12

66. Yanagisawa T, Shimizu T, Kuroda K, Kato C (1990) The preparation of alkyltriinethylaininonium kaneinite complexes and their

conversion to microporous materials. Bull Chem Soc Jpn 63:988 992

67. Yue Y, Gédéon A, Bonardet J L, J B D'E, Fraissard J, Melosh N (1999, 1967 1968) Direct synthesis of AlSBA mesoporous molec ular sieves: characterization and catalytic activities. Chem Commun

68. Zanjanchi M, Golmojdeh H, Arvand M (2009) Enhanced adsorp tive and photocatalytic achievements in removal of methylene blue by incorporating tungstophosphoric acid TiO2 into MCM 41. Journal of hazardous materials 169(1 3):233 239

69. Zhang Z et al (2001) Mesoporous aluminosilicates with ordered hexagonal structure, strong acidity, and extraordinary hydrothermal stability at high temperatures. J Am Chem Soc 123:5014 5021

70. Zhang S, Wang Z, Zhang Y, Pan H, Tao L (2016) Adsorption of methylene blue on organosolv lignin from rice straw. Procedia Environ Sci 31:3 11

71. Zhao G, Li C, Wu X, Yu J, Jiang X, Hu W, Jiao F (2018) Reduced graphene oxide modified NiFe calcinated layered double hydrox ides for enhanced photocatalytic removal of methylene blue. Appl Surf Sci 434:251 259